

Linkage between acoustic parameters and seabed sediment properties in the south-western Baltic Sea

Michael Endler · Rudolf Endler · Bernd Bobertz ·
Thomas Leipe · Helge W. Arz

Received: 12 August 2014 / Accepted: 8 January 2015 / Published online: 22 January 2015
© Springer-Verlag Berlin Heidelberg 2015

Abstract Acoustic profiling methods are widely used to provide a rapid view into geological structures. For the interpretation of acoustic profiling results (single- and multi-beam), reliable geo-acoustic models are needed. Suitable geo-acoustic models covering a wide range of sediment types do not exist to date for the Baltic Sea. Based on surface sediment datasets, geo-acoustic models have been set up for the prediction of acoustical parameters derived from sedimentological data for south-western Baltic Sea surface sediments. Empirical relationships were created to predict key in situ parameters (p-wave velocity, wet bulk density) from sedimentological core data, notably grain density and water content. The Gassmann-Hamilton equations were used to set up a more generic physically based model. For the first time semi-empirical equations for the calculation of the elastic frame modulus and the solid sediment particle modulus were established by an iterative Gassmann-Hamilton fitting procedure. The resulting models have a remarkably good performance with, for example, a calculated sound velocity accuracy of about 17–32 m s⁻¹ depending on model input data. The acoustic impedance of seafloor sediments can be estimated from single-beam echosounding if the contribution of seafloor reflectivity is extracted from the total acoustic signal. The data reveal a strong linkage between acoustic impedance and selected sediment properties (e.g. grain size, water content). This underlines the potential for effective mapping of seafloor sediment properties (e.g. habitat mapping). Furthermore, these geo-acoustic models can be used by marine geologists for a precise linkage between sediment facies identified in longer cores and

corresponding acoustic facies recorded by high-resolution seismic profiling in future work.

Introduction

Seismo-acoustic profiling methods are basic tools for the mapping of seafloor and sub-bottom sediments (Anderson et al. 2008). They deliver acoustic images of surface sediments and sub-bottom deposits, generating a quick view of seabed morphology and sedimentary structures. Both spatial and temporal characteristics of seabed sediments can be explored in this manner (e.g. Ostrovsky and Tegowski 2010), and seafloor classification methods can be applied to acoustic profiles obtained by, for example, side-scan sonar (e.g. Bartholomä 2006) or boomer seismics (Mendoza et al. 2014), on the basis of which bottom roughness and seafloor hardness can be estimated (e.g. Wöfl et al. 2014). However, acoustic images (be it vertical profiling obtained by, for example, sediment echosounders or horizontal profiling obtained by, for example, multi-beam echosounding) reflect only changes in acoustic impedance, which is defined as the product of wet bulk density and p-wave velocity. Therefore, the acoustic horizons do not necessarily indicate horizons or layers in the geological sense. In all cases the interpretation of acoustic profiles needs to be supported by ground truthing (e.g. sediment coring).

Acoustic sediment properties form the link between acoustic images and sedimentological characteristics of seafloor deposits. During the past 50 years, these have been studied intensively both in deep-sea and shelf regions, mainly in the course of various naval research projects (e.g. Joint High-Frequency Backscatter Experiment (JOBEX) and the Coastal Benthic Boundary Layer (CBBL) Program carried out by the Naval Research Laboratory, Washington, D.C.; e.g. Richardson and Bryant 1996). Edwin L. Hamilton

M. Endler (✉) · R. Endler · T. Leipe · H. W. Arz
Leibniz Institute for Baltic Sea Research,
18119 Warnemünde, Germany
e-mail: michael.endler@io-warnemuende.de

B. Bobertz
Ernst Moritz Arndt University, 17489 Greifswald, Germany

published numerous papers dealing with the acoustic characteristics of marine sediments from various environments worldwide (e.g. Hamilton et al. 1956; Hamilton 1980; Hamilton and Bachman 1982). The most recent and comprehensive collection of regressions for various world regions is contained in Jackson and Richardson (2007). A comparably small number of studies dealing with bottom sediment physical properties in the Baltic Sea are readily available from the international literature (e.g. Lu et al. 1998; Olea et al. 2008; Endler 2009), but these do not provide sufficient data for desired geo-acoustic models. Acoustic seabed classification has been carried out in the Baltic Sea using multi- or single-beam acoustic methods evaluating mainly processed backscattered signals (e.g. Tęgowski 2005; Orłowski 2007; see Parnum et al. 2009 for a comparison of multi- and single-beam echosounding).

In situ acoustic sediment properties are needed for precise merging of core data into acoustic profiles and their interpretation. Therefore, the sound velocity is the key parameter for the travel time-to-depth conversion of seismo-acoustic data. Both wet bulk density and sound velocity are required for the calculation of synthetic seismograms of sediment cores to identify acoustic and geological horizons. Seismic velocities can be obtained directly from multi-channel seismic data, but not from single-channel seismo-acoustic records. Therefore, the required acoustic core properties have to be obtained by either in situ measurements, sediment core logging or geo-acoustic modelling.

The term geo-acoustic modelling is used in the literature with two different meanings: (1) as the compilation of in situ sediment acoustic properties for a given area and defined sediment layers (independent of how the data were obtained), and (2) as the calculation of in situ acoustic properties for a coring station from its logging data and/or sedimentological parameters. In this paper both approaches are combined for the determination of in situ acoustic properties for coring stations based on empirical regression functions, and a physically based model.

Numerous physically based geo-acoustic theories existing to date were grouped by Jackson and Richardson (2007) into fluid, elastic and poroelastic approaches. The names of these approaches indicate the properties of the medium in which the acoustic wave propagation is investigated. While fluid theories are preferably used in modelling acoustic wave propagation in the water column, elastic and poroelastic approaches dominate in geophysics (Mavko et al. 1999). The main difference between elastic and poroelastic approaches is that poroelastic models accommodate the motion between the solid frame of the porous medium and the pore water, and the elastic theories do not. Poroelastic models are considered to be more realistic, but they become much more complex than elastic approaches. The most prominent poroelastic theory was developed by Biot (1956a, 1956b, 1962). The Biot theory

was extended by many authors such as Stoll (1974, 1989), Dvorkin and Nur (1993), Leurer (1997), and Chotiros and Isakson (2004). An increased number of input parameters of about 13 is one of the major difficulties for the effective application of these models. Therefore, this paper investigates a relatively simple elastic model to derive functions for the calculation of elastic parameters needed in both elastic and poroelastic models. This work is crucial for the design of an improved practicable Biot model for future work.

Within this context, the acoustic impedance (= wet bulk density * p-wave velocity) of seabed sediments is essential for the processing and interpretation of seismo-acoustic profiling records. The aim of this study is to investigate the relationships between acoustical parameters and characteristic sedimentological properties in the south-western Baltic Sea within the framework of the physical Gassmann-Hamilton model (Gassmann 1951; Hamilton 1971a, 1971b).

Physical setting

The study area comprises two western Baltic Sea basins, i.e. Mecklenburg Bay and the Arkona Basin (Fig. 1) connecting the Danish straits with the Baltic Proper. All water masses entering and leaving the Baltic Sea pass this area, with approx. $470 \text{ km}^3 \text{ year}^{-1}$ of salt-rich water flowing in near the bottom from the North Sea and approx. $665 \text{ km}^3 \text{ year}^{-1}$ of lower-salinity water flowing out in surface waters via the Danish straits (<http://www.io-warnemuende.de/steckbrief-der-ostsee.html>). Thus, stratification of the water column is quite common but, in contrast to the deeper basins of the Baltic, laminated sediments cannot be expected because bottom anoxic conditions are short-lived and bioturbation prevalent. Salinity varies seasonally between 10 and 20 psu in bottom waters (Krauss and Brüggel 1991; Liljebladh and Stigebrandt 1996; Lass and Mohrholz 2003).

Mecklenburg Bay has a maximum depth of roughly 28 m whereas the Arkona Basin is about 40–50 m deep. The two basins are separated by the Darss Sill. The Arkona Basin has a relatively smooth morphology as a result of late and post-glacial basin filling with muddy and sandy sediments (Lemke 1998). Detailed information about western Baltic Sea development can be found in Eronen et al. (1990), Jensen (1995), Jensen et al. (1997), Lemke (1998) and Andrén et al. (2000). The central sector is filled with greenish soft organic-rich mud, the organic material originating both from in situ primary production and terrestrial input (e.g. via the Oder River; Miltner and Emeis 2000). The basin is surrounded by the Adlergrund and Kriegers Flak where sandy sediments characterise shallower depths at 10–20 m. The surface sediments of Mecklenburg Bay consist of greenish grey mud with increased sand contents towards the coastal zone.

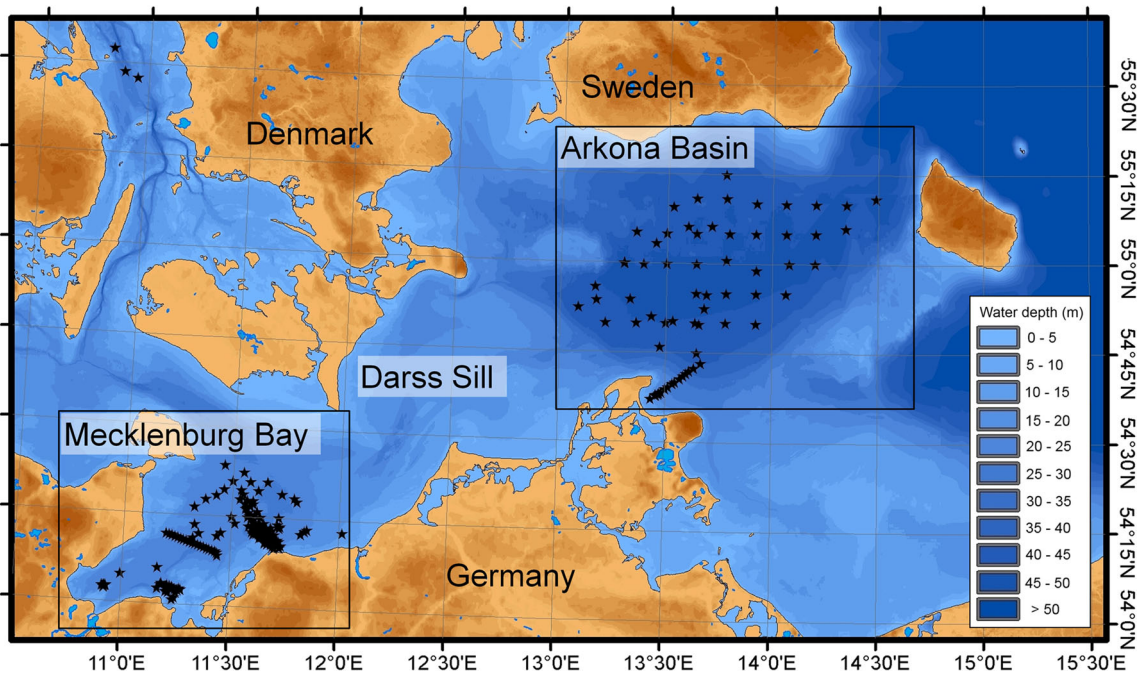


Fig. 1 The south-western Baltic Sea, showing the main study areas with sampling stations in Mecklenburg Bay and the Arkona Basin

The Trave River supplies only a minor amount of sediments to the bay.

Materials and methods

Main sampling and processing

The integrated dataset comprises both sedimentological and acoustical data for each sample. The youngest samples were obtained during IS-SediLab cruise EMB1218 (2012, 14 stations, 179 sub-samples) and IS-SediLab cruise EMB058 (2013, 12 stations, 108 sub-samples), expanding on extensive archive data (226 stations, 1,790 sub-samples) gathered during the years 2000 to 2010 by the Leibniz Institute for Baltic Sea Research Warnemünde (IOW).

Samples were obtained with either a multi-corer (MUC) or a Frahm corer (FC) covering depths up to 81 cm but on average 23 cm. The cores were stored vertically and subsequently also logged vertically with a vertical core logger (see below). This paper is based on data from 2,077 sub-samples from 252 stations, the key parameters being listed in Table 1. In order to cover as many sediment types as possible, the Mecklenburg Bay and Arkona Basin datasets were extended with additional samples from the Kattegat (five stations), the Danish straits (three stations) and the northern Bornholm Basin (four stations).

Considering the relevance for acoustic profiling, the 0–15 cm depth interval was defined as “surface sediments”, in each case comprising 2–5 samples and ensuring statistical

reliability by averaging their sediment characteristics over depth and time. These uppermost sediments are mostly very weakly consolidated and dominated by self compaction, and are particularly important for high-frequency (>10 kHz) acoustic profiling with wavelength <0.2 m. Lower-frequency acoustic profiling (<10 kHz, wavelength >0.2 m) and the expected influence of overburden pressure compaction were accommodated in another dataset spanning the 0–40 cm depth interval.

Table 1 List of parameters and abbreviations

Measured data	Calculated data
d_s (kg m^{-3}): grain density	G (Pa): elastic shear module
GsQ50phi: median grain size (phi)	dbd (kg m^{-3}): dry bulk density
LOI (-): fractional loss on ignition	d_w (kg m^{-3}): density of water
M_b (kg): mass of bulk sediment	K_f (Pa): elastic bulk modulus of frame
M_w (kg): mass of pore water	K_s (Pa): solid bulk modulus of particles
S (psu): salinity of pore water	por (-): fractional porosity
T ($^{\circ}\text{C}$): temperature of bulk sediment	V_p (m s^{-1}): p-wave velocity
	V_{pR} (-): p-wave velocity ratio
	V_s (m s^{-1}): shear wave velocity
	wbd (kg m^{-3}): wet bulk density
	wc (-): fractional water content
	Z_{ac} ($\text{kg m}^{-2} \text{s}^{-1}$): acoustic impedance
	ZR (-): acoustic impedance ratio

Physicochemical parameters

Pore water salinity was determined with a conductivity meter from Omnilab (WTW LF537). Pore water samples were obtained by centrifuging bulk sediment sub-samples in a Sigma 3K12 centrifuge for 10 minutes at 4,000 revolutions per minute.

The mass of each fresh, water-saturated bulk sediment sample (M_b) was determined immediately after sub-sampling. Then, the fresh samples were freeze dried with a Christ Alpha 1-4 (vacuum 0.37 bar, ice condenser $-54\text{ }^\circ\text{C}$, plate heating $+30\text{ }^\circ\text{C}$) for 3 days. Determining the mass of the dry samples enabled calculating the mass of the pore water (M_w).

The salinity (S)-corrected *absolute water content* (wc) was calculated as (cf. Hamilton 1971b):

$$wc = \frac{M_w}{M_b (1-S)} \quad (1)$$

For determination of *grain density* (d_s), 50 ml pycnometers were filled with ca. 3–9 g of dried sediment and deionised water, followed by degassing overnight in an exsiccator at 0.1 mbar (cf. Manheim et al. 1974; Schwartz 1985; Yang 2004; German DIN18124 2011). Consistent with ever-increasing evidence for gas-charged sediments in the Baltic Sea region (e.g. Mogollón et al. 2013; Ulyanova et al. 2014), particularly the muddy sediment samples and, for that matter, the deionised water itself contained measurable amounts of gas that had to be decompressed, resulting in a rather time-consuming procedure. d_s was calculated as:

$$d_s = \frac{m_s}{V_{py} - m_{pyws} - m_{pys}} \cdot \frac{1}{\rho_w} \quad (2)$$

where m_s is the mass of the dried sample, V_{py} the volume of the pycnometer, m_{pyws} the mass of the pycnometer + water + sediment, m_{pys} the mass of the pycnometer + sediment, and ρ_w the density of water at a given temperature.

Wet bulk density (wbd) was calculated from the fractional water content, grain density and pore water density (d_w , calculated using the Matlab toolbox SEAWATER Library Version 1.2e of Morgan 1998):

$$wbd = \frac{d_s \cdot d_w}{wc \cdot d_w + (1-wc) \cdot d_w} \quad (3)$$

Dry bulk density (dbd) was calculated as:

$$dbd = \frac{(1-wc) \cdot d_s \cdot d_w}{(wc \cdot d_s + (1-wc) \cdot d_w)} \quad (4)$$

and fractional *porosity* (por) as:

$$por = \frac{d_s \cdot wc}{wc \cdot d_s + (1-wc) \cdot d_w} \quad (5)$$

Grain size analyses were carried out using a CILAS 1180 Lasersizer for grain sizes of 0.3 to 2,000 μm . The dried sediments (0.07–0.15 g) were suspended in 30 ml deionised water + 10 ml 35% H_2O_2 + 3 ml sodium polyphosphate, followed by 15 minutes of ultrasonic treatment and storage for 24 h before measuring. Although the pre-treatment with oxidizing chemicals is not optimal, it was dictated by the aim to compare with similarly treated archive data. Larger particles ($>2\text{ mm}$) were dry-sieved with a RETSCH easy sieve.

Loss on ignition (LOI) was determined by heating the dried samples at $550\text{ }^\circ\text{C}$ for 3 h. The loss of mass subdivided by the initial mass gives the fractional LOI or fractional organic matter content; commonly, these values are expressed as percentages. In the present case, the total organic carbon (TOC) content could then be derived as $\text{TOC} (\%) = \text{LOI} (\%) / 2.8$, based on data for western Baltic Sea surface sediments from Leipe et al. (2011).

p-wave velocity

For the archival cores, a standard GEOTEK multi sensor core logger (MSCL) was used for *p*-wave velocity measurements. The MSCL was designed for full core logging with two rolling contact transducers (cf. no contact fluid is needed) operating at a central frequency of 230 kHz at a down-core depth interval of 5 mm. The *p*-wave sensor of the MSCL uses a pulse travel method combined with a zero crossing detection electronic module for travel time estimation. This method works very well for sediments with low absorption and minor signal distortion. Otherwise, *p*-wave velocity errors can reach about 100 m s^{-1} (e.g. for a travel time detection error of one period, 230 kHz, sediment core thickness 0.1 m). These errors were eliminated by independent gamma density data. For more information, the reader is referred to www.geotek.co.uk and Blum (1997).

The short cores of the IS-SediLab expeditions were logged with a new vertical core logger (VCL) designed at IOW. A sensor head is placed on top of the sediment-containing core liner. Then, the sediment core is pushed stepwise through the sensor head, and *p*-wave velocity, temperature, *p*-wave attenuation, electrical conductivity and magnetic susceptibility are measured. During the logging procedure, the core is sliced in slabs of 2 cm thickness for further analyses.

Compared to the MSCL, some general advantages of this new logger are that the core is logged in a vertical position and the sediment surface is much less disturbed, which enables measurement of the water–sediment transition; moreover,

the sensors are in direct contact with the sediment sample and therefore there is no influence of the liner material. p-wave velocity is measured by a pulse transmission method. The piezoceramic transducers are driven at frequencies of 1 MHz and 430 kHz. The driving voltage is automatically adapted to the received signal level in order to match the dynamic range of the analog to digital (AD) converter. A set of measurements performed with seawater of known salinity is used for calibration. Pulse travel time is estimated by correlating the received pulse with the calibration reference pulse. The correlation method gives better results for sediments with high sound absorption and is in general more robust against smaller signal distortion than the zero crossing method. Data calibration and data cleaning (cf. outliers) is performed in a final VCL processing procedure, whereby the reliability of the measured p-wave velocity data is estimated using p-wave velocity predictions obtained from sample wet bulk density data.

XRF scanning and SEM/EDX analyses

Elemental composition was assessed by XRF scanning. Dried sample material was analysed with an ITRAX core scanner from COX Analytics, using a chromium tube to determine Al, Si, S, K, Ca, Ti, Mn, Fe, Zr, and Ba at 30 kV and 30 mA at 15 s point and 2.5 mm intervals.

Based on a cluster analysis (see below), a representative sample was selected from each of four classes for SEM/EDX-based mineralogical analyses by means of a MERLIN VP compact (Carl Zeiss) scanning electron microscope (SEM) equipped with an AZtecEnergy (Oxford Instruments) energy dispersive X-ray spectroscopy (EDX) unit. The system used for single particle micro-analyses is new but the general procedure is described in Leipe et al. (1999).

The samples were prepared on Nucleopore filters, stacked on aluminium stubs and coated with carbon for EDX. Particles between 0.6 and 90 μm were measured for 12 elements (Na, Mg, Al, Si, P, S, Cl, K, Ca, Ti, Mn, Fe) classified as quartz, opal, calcite, albite, plagioclase, potassium feldspar, kaolinite, illite, illite-mixed layer, smectite, chlorite, Mg-, K-, Fe- clay minerals, barite, pyrite, dolomite, bauxite, titanium minerals, Fe-oxides, Mn-oxides, CaPO_4 , Mn-Fe- PO_4 and organic matter, the latter defined in terms of its minor elemental spectrum (Si, P, S).

Results

Empirical functions

The sedimentological dataset from the south-western Baltic Sea served to generate regression functions for the calculation of wet bulk density, p-wave velocity

and, accordingly, acoustic impedance for both the 0–15 and 0–40 cm depth intervals (see above) using Matlab scripts (Figs. 2, 3, 4 and 5, Tables 2 and 3). The analyses started with dependencies for a single variable. Metric units were used for the independent variables, with the exception of the grain size data for which a phi scale was chosen (Krumbein 1938), since usually these show a log-normal distribution. Several fitting functions were tested. Frequently, the hyperbolic tangent functions resulted in better predictions for values outside the data range of the independent variable than did the commonly used polynomials. Polynomial functions gave best fits only for p-wave velocity. The standard deviation of the differences between the observations and predictions was calculated as a measure of the fitting error. Fitting procedures tested on two dependent variables (multiple regression) lead to no useful results.

The equations in Table 2 enable the calculation of wet bulk density, porosity and water content from loss on ignition and median grain size. Since water content and porosity are strongly correlated, not all regressions are illustrated as graphs.

Because p-wave velocity is sensitive to the temperature, salinity and pressure of the pore water, it is common practice to use the p-wave velocity ratio instead. This ratio is normalised to pore water properties (salinity, temperature), i.e. the measured sound velocity is divided by the corresponding pore water p-wave velocity. The latter was calculated for the laboratory measurement conditions and pore water salinity using the Matlab toolbox of Morgan (1998).

Gassmann-Hamilton model

Hamilton (1971b) used a physically based geo-acoustic elastic model where the velocities of compressional (pressure/longitudinal) waves V_p and shear (transversal) waves V_s in a homogeneous medium can be calculated from the elastic (dynamic) modulus and wet bulk density:

$$V_p = \sqrt{\frac{K_b + 4/3G}{\text{wbd}}} \quad (6)$$

$$V_s = \sqrt{\frac{G}{\text{wbd}}} \quad (7)$$

where K_b (Pa) is the compressional bulk modulus and G (Pa) the dynamic shear modulus of the wet bulk sediment.

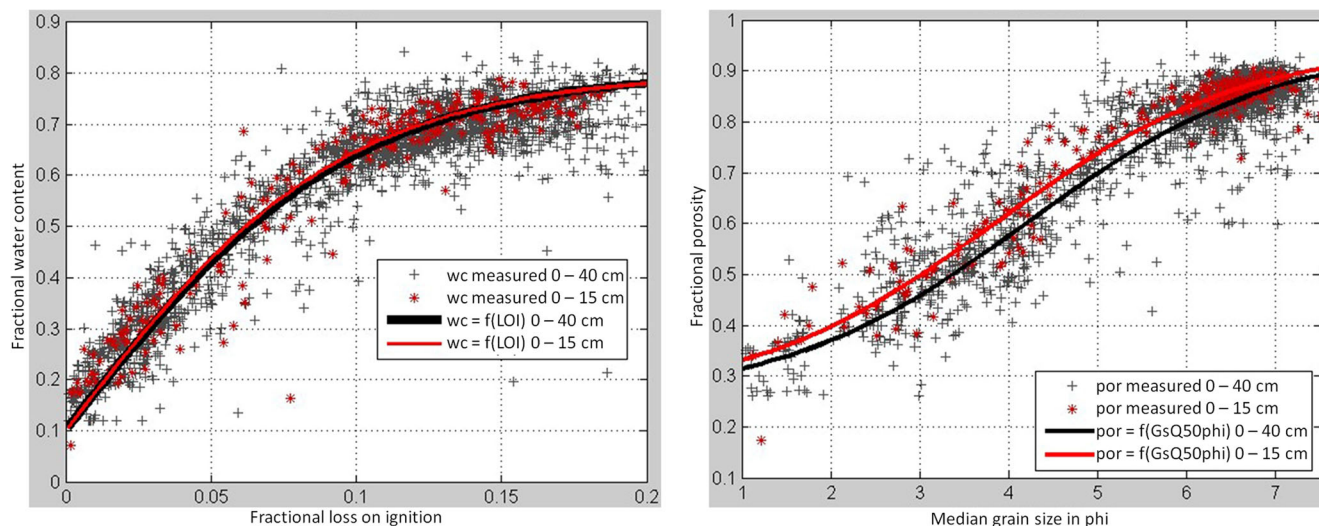


Fig. 2 Fractional water content as function of fractional loss on ignition (*left*) and median grain size (*right*, phi scale)

Gassmann (1951) developed a set of equations to calculate K_b from the bulk moduli of the following sediment constituents: K_w of the pore water, K_s of the solid particles, K_f of the solid frame, and the porosity por:

$$K_b = K_s \frac{K_f + Q}{K_s + Q}, \quad Q = \frac{K_w (K_s - K_f)}{\text{por} (K_s - K_w)} \quad (8)$$

These input parameters are a subset of those needed for an improved Biot model. The *dynamic shear modulus* of the wet bulk sediment, G , can be obtained from the shear velocity V_s using Eq. 7:

$$G = V_s^2 \cdot \text{wbd} \quad (9)$$

Shear velocity, V_s , was calculated based on Jackson and Richardson (2007):

$$V_s = 692 \cdot e^{(-4.94 \cdot \text{por})} \quad (10)$$

The *compression modulus of the pore water*, K_w , can be calculated from its density d_w and its sound velocity V_{pw} using Eq. 6 and setting $G=0$; pore water density $d_w = f(S, T, P)$ and p-wave velocity $V_{pw} = f(S, T, P)$ were calculated based on Morgan (1998):

$$K_w = V_{pw}^2 \cdot d_w \quad (11)$$

The estimates of K_f and K_s were generated by nonlinear fitting procedures. Based on logical considerations, the

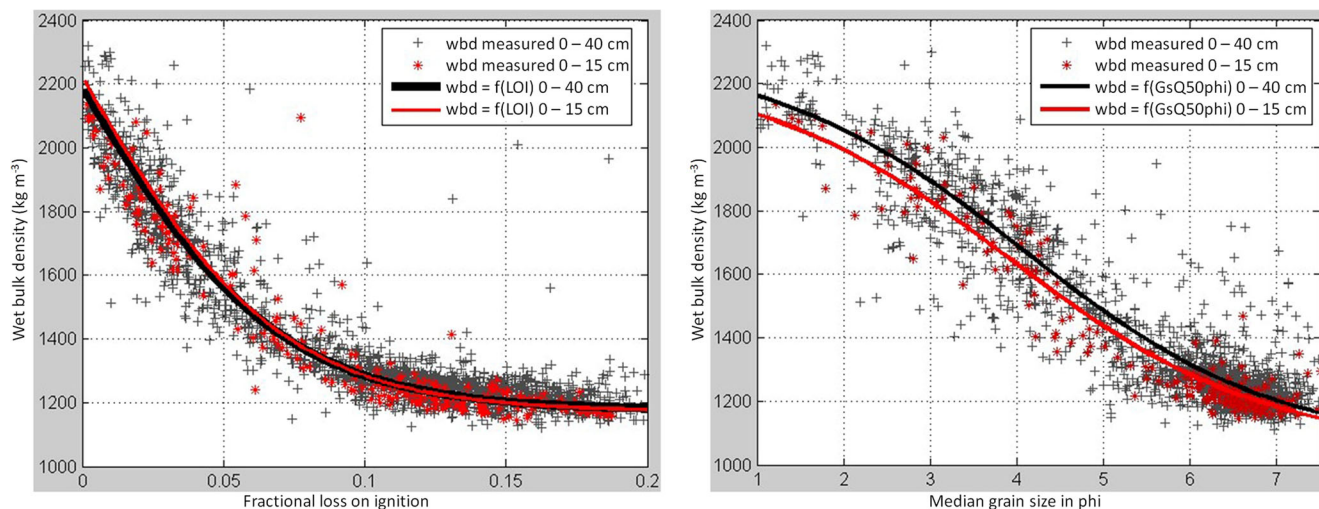


Fig. 3 Wet bulk density as function of fractional loss on ignition (*left*) and median grain size (*right*, phi scale)

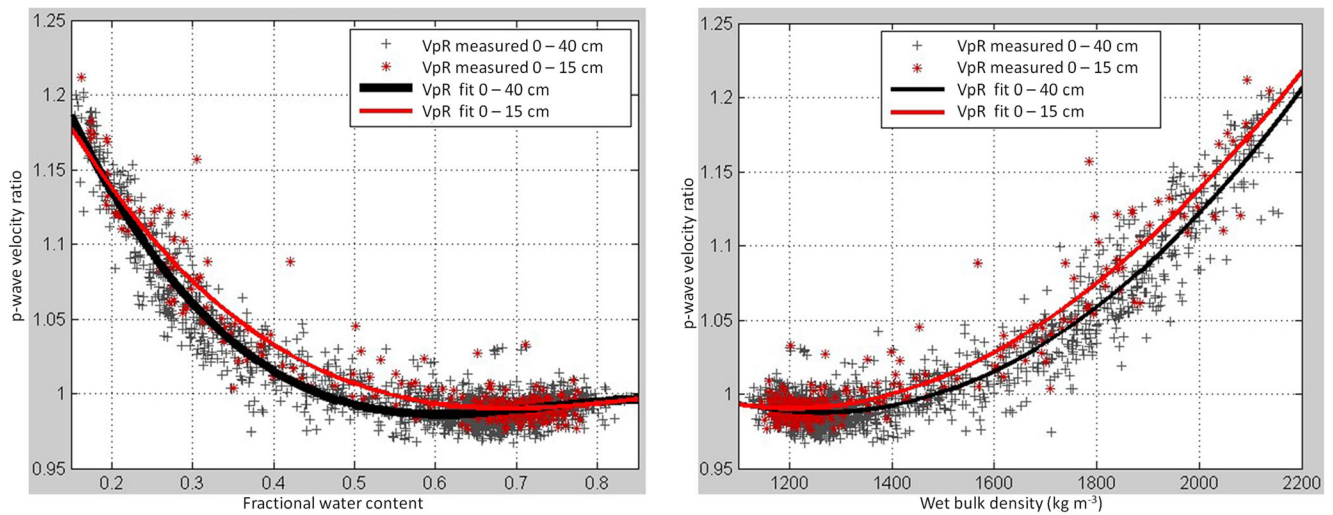


Fig. 4 p-wave velocity ratio as function of fractional water content (*left*) and wet bulk density (*right*)

compression modulus of the solid frame K_f should be a function of porosity. The estimated grain density reflects the mineral composition and organic matter content, and may be used for the calculation of K_s . Initial trials confirmed the general dependencies $K_f = f(\text{por})$ and $K_s = f(d_s)$; corresponding fitting formulae are reported in Table 4.

The Gassmann-Hamilton model and the $K_f = f(\text{por})$ and $K_s = f(d_s)$ formulae were used in a nonlinear fitting procedure to estimate the constants of the K_f and K_s fitting functions and to predict p-wave velocities. The measured water content, grain density, as well as salinity and temperature of the pore water were the basic input parameters. Other derived input parameters such as porosity and wet bulk density were obtained from Eqs. 1 to 5. The results are depicted in the left-hand panel of Fig. 6. p-wave velocity was corrected to 20 °C and 20 psu pore water salinity in order to compare the data with the regression model of Jackson and Richardson

(2007) and the regression of the 0–40 cm Baltic Sea basic dataset (see Table 5). The differences (standard deviation) between p-wave velocity prediction and measurement are 17.0 m s⁻¹ for the Gassmann-Hamilton model, 17.4 m s⁻¹ for the Baltic Sea data regression, and 19.7 m s⁻¹ for the Jackson and Richardson (2007) regression.

Changes in environmental conditions such as temperature, depth and salinity were taken into account in the Gassmann-Hamilton model by the pore water properties, mainly the compression modulus and, to a lesser extent, the density. Therefore, one advantage of the Gassmann-Hamilton model is that p-wave velocities can be calculated directly for the desired S, T, P environmental conditions. Using regression models like those described above, these in situ corrections were obtained by the sound velocity ratio and the pore water properties.

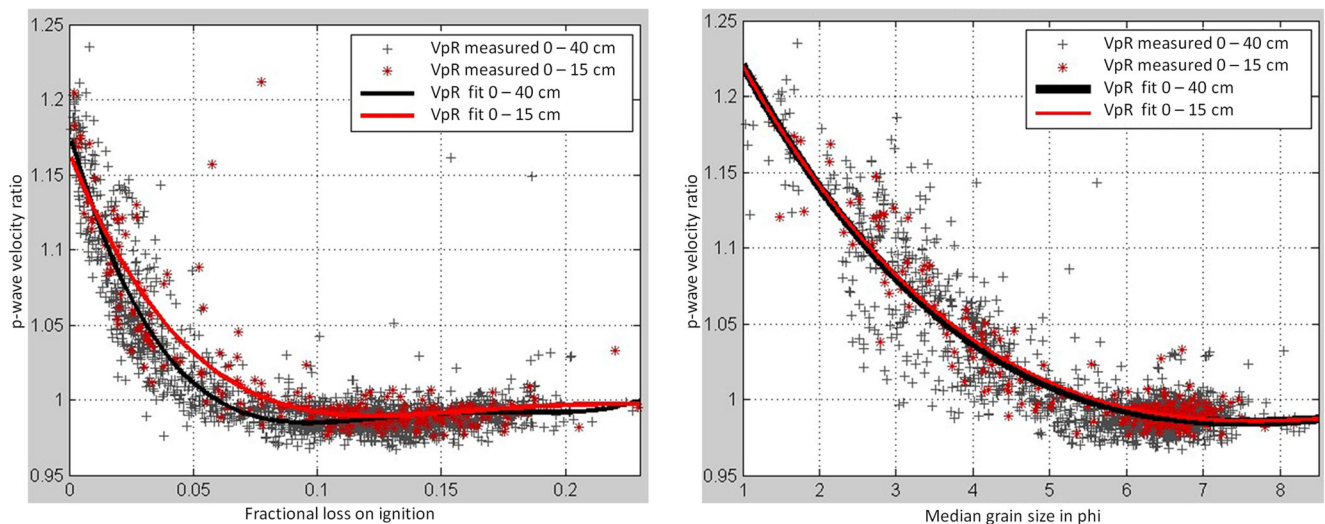


Fig. 5 p-wave velocity ratio (VpR) as function of fractional loss on ignition (*left*) and median grain size (GsQ50phi, phi scale, *right*)

Table 2 Volume/mass-related regression functions and parameters for the 0–15 and 0–40 cm datasets

Regression functions	Standard deviation (measured vs. calculated); range of validity
0–15 cm dataset	
wbd (kg m ⁻³) = 1170 + 1050 • [1.0 - tanh($\frac{LOI}{0.22} \cdot \pi$)]	77 (kg m ⁻³); LOI: 0–0.25
wbd (kg m ⁻³) = 1050 + 600 • {1.0 - tanh[- π + ($\frac{GsQ50phi}{18.5}$ + 0.29) • 2 π]}	77 (kg m ⁻³); GsQ50phi: 1–8 phi
por (-) = 0.32 + 0.58 • [tanh($\frac{LOI}{0.23} \cdot \pi$)]	0.046 (-); LOI: 0–0.2
por (-) = 0.25 + 0.35 • {1.0 + tanh[- π + ($\frac{GsQ50phi}{17.5}$ + 0.28) • 2 π]}	0.055 (-); GsQ50phi: 1–8 phi
wc (-) = 0.1 + 0.7 • [tanh($\frac{LOI}{0.3} \cdot \pi$)]	0.059 (-); LOI: 0–0.2
wc (-) = 0.101 + 0.35 • {1.0 + tanh[- π + ($\frac{GsQ50phi}{14.5}$ + 0.2) • 2 π]}	0.055 (-); GsQ50phi: 1–8 phi
0–40 cm dataset (regression functions differing from those of 0–15 cm dataset)	
wbd (kg m ⁻³) = 1050 + 625 • {1.0 - tanh[- π + ($\frac{GsQ50phi}{18.5}$ + 0.28) • 2 π]}	102 (kg m ⁻³); GsQ50phi: 1–8 phi
por (-) = 0.25 + 0.35 • {1.0 + tanh[- π + ($\frac{GsQ50phi}{17.5}$ + 0.26) • 2 π]}	0.073 (-); GsQ50phi: 1–8 phi
wc (-) = 0.101 + 0.35 • {1.0 + tanh[- π + ($\frac{GsQ50phi}{14.5}$ + 0.18) • 2 π]}	0.073 (-); GsQ50phi: 1–8 phi

Based on the Gassmann-Hamilton model, p-wave velocities were calculated for a porosity range of 0.2 to 1.0, temperature of 20 °C, pore water salinity of 20 psu (VpGH20-20), and for the same porosity range at 10 °C and 10 psu (VpGH10-10, see below). In order to test the widely used p-wave velocity ratio method, another 10 °C, 10 psu velocity dataset was obtained from VpGH20-20 by multiplication with the pore water velocity ratio VpPf10-10 / VpPf20-20. The results are plotted in the right-hand panel of Fig. 6. The velocity differences obtained are in the range of 42–57 m s⁻¹, which is a non-negligible in situ correction. The porosity dependence of the velocity difference for both methods can be seen clearly. The Gassmann-Hamilton model difference is about 4 m s⁻¹ less than the velocity ratio method, and has a minimum at a porosity of about 0.7. The velocity differences of both methods of 4 m s⁻¹ are negligible for most practical applications.

The elastic moduli of the frame K_f and of the solid particles K_s are the most complicated and critical input parameters of the Gassmann-Hamilton model (and also the Biot-Stoll model (Biot 1956a, 1956b, 1962; Stoll 1974). Rearranging Gassmann's Eq. 8 for the frame bulk modulus K_f yields:

$$K_f = \frac{K_b (\text{por} (K_s - K_w) + K_w) - K_w \cdot K_s}{\text{por} (K_s - K_w) + K_w \left[\left(\frac{K_b}{K_s} \right) - 1 \right]} \quad (12)$$

Solving Eq. 8 for K_s leads to a quadratic equation:

$$a \cdot K_s^2 + b \cdot K_s + c = 0 \quad (13)$$

with

$$a = \text{por} (K_b - K_f) - K_w$$

Table 3 Sound velocity ratio regression functions and parameters for the 0–15 and 0–40 cm datasets

Regression functions	Standard deviation (measured vs. calculated); range of validity
0–15 cm dataset	
VpR = 1.34 - 1.26 • wc + 1.49 • wc ² - 0.55 • wc ³	0.013 (-) ≈ 19 m s ⁻¹ ; wc: 0.15–0.8
VpR = 1.32 - 0.36 • por - 0.48 • por ² + 0.51 • por ³	0.011 (-) ≈ 17 m s ⁻¹ ; por: 0.35–0.9
VpR = 1.39 - 6.9 • 10 ⁻⁴ • wbd + 3.26 • 10 ⁻⁷ • wbd ² + 2.13 • 10 ⁻¹¹ • wbd ³	0.012 (-) ≈ 17 m s ⁻¹ ; wbd: 1,100–2,200 kg m ⁻³
VpR = 1.32 - 0.11 • GsQ50phi + 0.012 • GsQ50phi ² - 4.29 • 10 ⁻⁴ • GsQ50phi ³	0.012 (-) ≈ 18 m s ⁻¹ ; GsQ50phi: 1–8 phi
VpR = 1.16 - 4.09 • LOI + 34.02 • LOI ² - 119.13 • LOI ³ + 151.19 • LOI ⁴	0.021 (-) ≈ 32 m s ⁻¹ ; LOI: 0–0.2
0–40 cm dataset	
VpR = 1.40 - 1.78 • wc + 2.49 • wc ² - 1.12 • wc ³	0.011 (-) ≈ 19 m s ⁻¹ ; wc: 0.15–0.8
VpR = 1.61 - 1.69 • por + 1.38 • por ² - 0.30 • por ³	0.011 (-) ≈ 17 m s ⁻¹ ; por: 0.35–0.9
VpR = 1.36 - 5.8 • 10 ⁻⁴ • wbd + 2.18 • 10 ⁻⁷ • wbd ² + 6.25 • 10 ⁻¹² • wbd ³	0.012 (-) ≈ 18 m s ⁻¹ ; wbd: 1,100–2,200 kg m ⁻³
VpR = 1.32 - 0.12 • GsQ50phi + 0.013 • GsQ50phi ² - 4.46 • 10 ⁻⁴ • GsQ50phi ³	0.017 (-) ≈ 26 m s ⁻¹ ; GsQ50phi: 1–8 phi
VpR = 1.17 - 5.76 • LOI + 61.63 • LOI ² - 278.09 • LOI ³ + 453.91 • LOI ⁴	0.016 (-) ≈ 25 m s ⁻¹ ; LOI: 0–0.2

Table 4 Fitting functions for elastic frame and solid grain bulk moduli

Fitting functions for all data	Standard deviation (measured vs. calculated)
K_f (Pa) = $1.8472 \cdot 10^9 \cdot (1 - \text{por})^{1.3638}$	$1.269 \cdot 10^8$ Pa; por: 0.3–0.9
K_s (Pa) = $9.538 \cdot 10^9 - 9.460 \cdot 10^8 \cdot \frac{d_s - 2075}{3518} + 4.217 \cdot 10^{10} \cdot \{1 + \tanh[\pi - (1 - \frac{d_s - 2075}{3518}) \cdot 2\pi]\}$	$9.923 \cdot 10^{11}$ Pa; d_s : 2,200–2,900 kg m ⁻³

$$b = K_w [K_b + K_f + \text{por} (K_b + K_f)]$$

$$c = K_b \cdot K_w \cdot K_f$$

Then, K_s is given by:

$$K_s = -\frac{b}{2 \cdot 1} - \sqrt{b^2 - 4 \cdot a \cdot c} \tag{14}$$

Equations 12 and 13 served to calculate the frame and solid grain bulk moduli. The compressional bulk modulus of the wet bulk sediment K_b was obtained from Eqs. 6, 9, 10, 11 and 12. For the remaining unknown variable, the corresponding fitting function for K_f or K_s (obtained by the abovementioned Gassmann-Hamilton nonlinear fitting procedure) was used. The results are depicted in Fig. 7. Black asterisks indicate the bulk moduli obtained from Eqs. 12 and 13, which can be considered as “measured” data. Red circles show the run of the fitting functions (see

Table 4). Blue squares depict values for K_f and K_s from the literature (K_f values from Hamilton 1971b, K_s values of single minerals from Jackson and Richardson 2007). The K_f and K_s values of the “measured” data and of the fitting functions seem realistic and agree fairly well with the corresponding literature data. The scattering of the “measured” data points around the fitting functions is rather high. The reason for this presumably lies in the more complex K_f and K_s dependencies, although checks of the fitting function (“measured”) data against other parameters (e.g. grain size) did not lead to useful results. Another reason might be the higher sensitivity of the K_f , K_s formulae (Eqs. 12, 13) in terms of errors in the input parameters, especially K_b and the underlying p-wave velocities. Nevertheless, the fitting functions obtained for K_f and K_s work very well in the Gassmann-Hamilton model (cf. above) for the prediction of p-wave velocities.

Acoustic impedance for prediction of sediment properties

In the case of a plane acoustic wave incident upon a plane seafloor surface, i.e. for normal incidence, the plane wave

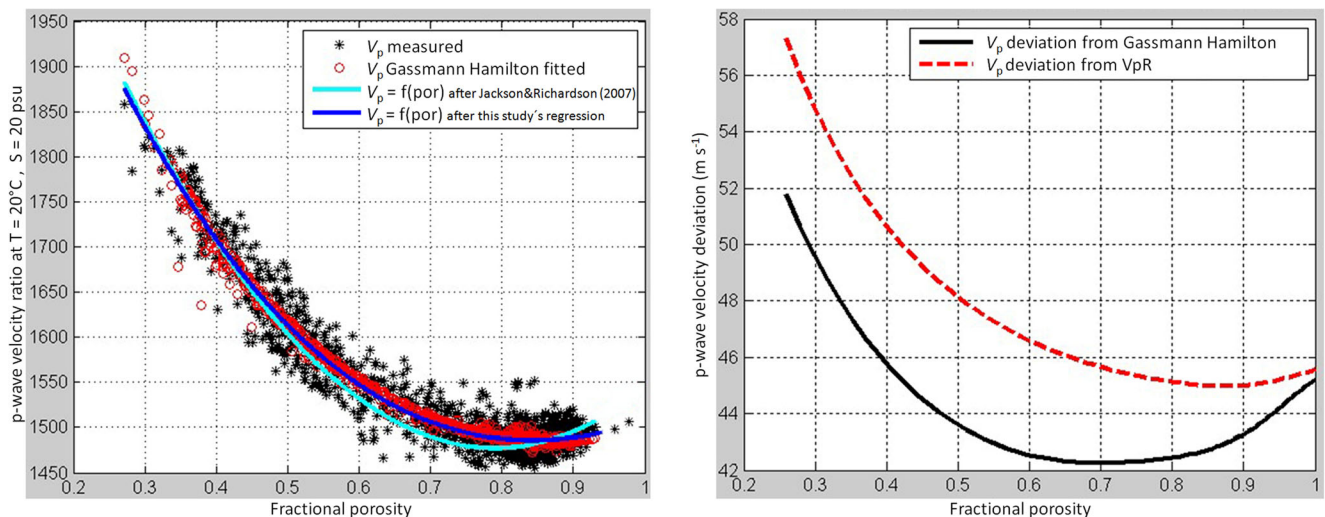


Fig. 6 Left Measured p-wave velocity at 20 °C, 20 psu salinity vs. fractional porosity for the 0–40 cm Baltic Sea dataset (asterisks; blue line regression) and corresponding predictions based on the Gassmann-Hamilton model (red circles) and the Jackson and Richardson (2007) model (turquoise line). Right Gassmann-Hamilton model-based influence

of pore water properties on p-wave velocity vs. porosity: black line difference between p-wave velocities calculated at 20 °C, 20 psu and at 10 °C, 10 psu; red line 10 °C, 10 psu velocities derived from 20 °C, 20 psu velocities by multiplication with the corresponding velocity ratio. For more information, see main text

Table 5 Derived empirical functions for the prediction of sedimentological properties from acoustic impedance ratio ZR (valid only for normal incidence, and not accounting for bedforms and benthic life; range of validity is 1.1–2.6 for ZR)

Regression functions	Standard deviation (measured vs. calculated)
0–15 cm dataset	
wc (-)=4.23–5.25•ZR+2.36•ZR ² –0.36•ZR ³	0.019
por (-)=1.94•e ^{-0.69•ZR} +0.027•ZR ^{0.027}	0.016
wbd (kg m ⁻³)=1010+1253•log(0.995•ZR)	15.9 kg m ⁻³
dbd (kg m ⁻³)=1972•log(1.0048•ZR)	24.5 kg m ⁻³
VpR (-)=1.43–0.82•ZR+0.46•ZR ² –0.07•ZR ³	0.01
LOI (-)=-1259•e ^{-5.75•ZR} +4.9•ZR ^{4.9}	0.030
GsQ50phi=19.98•e ^{-0.94•ZR} -0.003•ZR ^{-0.003}	0.52 phi
0–40 cm dataset (regression functions differing from those of 0–15 cm dataset)	
wc (-)=3.88–4.64•ZR+2.03•ZR ² –0.31•ZR ³	0.016
wbd (kg m ⁻³)=1010+1221•log(0.997•ZR)	15.8 kg m ⁻³
VpR (-)=1.39–0.78•ZR+0.46•ZR ² –0.07•ZR ³	0.01
LOI (-)=-374•e ^{-5.40•ZR} +2.2•ZR ^{2.2}	0.026
GsQ50phi=17.66•e ^{-0.83•ZR} -0.003•ZR ^{-0.003}	0.58 phi

reflection coefficient R is defined as (Lurton 2002):

$$R = \frac{Z_b - Z_w}{Z_b + Z_w} = \frac{Z_b/Z_w - 1}{Z_b/Z_w + 1} = \frac{ZR - 1}{ZR + 1} \quad (15)$$

where Z_b is the acoustic impedance of the bulk sediment (i.e. $wbd \cdot V_p$), Z_w the acoustic impedance of pore water, and $ZR = Z_b/Z_w$ the acoustic impedance ratio of the two media. R can be derived from acoustic profiling data. The acoustic impedance ratio is obtained by rearranging Eq. 15:

$$ZR = \frac{1 + R}{1 - R} \quad (16)$$

The Baltic Sea surficial sediment dataset served to examine empirical relations for the prediction of sedimentological parameters from acoustic impedance. Wet bulk density and p-wave velocity are sensitive to pore water salinity, temperature and pressure. Therefore, the acoustic impedance ratio $ZR = Z_b/Z_w$ was used for this purpose, rather than Z_b , the acoustic impedance of the surface sediment. Z_w is the acoustic impedance of the sample pore water under laboratory conditions. Density and p-wave velocity of the pore water were calculated

based on Morgan (1998). Depending on the scatter plots of the variables, different curve fitting function types were tested, using Matlab fitting procedures like “polyfit” and “nlinfit”. Results are depicted in Figs. 8, 9 and 10.

For the $wc = f(ZR)$ dependency (see Fig. 8, left-hand panel), an exponential function was not applicable, although the distribution of measured data implies such a function. A third-degree polynomial best matches the data, but it underestimates water contents exceeding the given validity range. All curve fitting procedures were performed on the two datasets described above, i.e. the 0–15 and the 0–40 cm depth intervals. In the figures, red asterisks and black crosses indicate the measured values of the 0–15 and the 0–40 cm depth intervals respectively. In each case, the run of the fitting functions is plotted on top of the measured data (red and black lines respectively). The differences between all predicted and measured values were calculated for each predicted sediment parameter. The standard deviation of these differences indicates offsets and errors of the predictions. The fitting functions and their parameters are listed in Table 5.

Sediment classification and spatial distribution

Statistical analyses were performed for classification of the dataset, capturing lateral distribution patterns, and to develop a method for depth-dependent (longer core) sediment discrimination for future work. Classification was in terms of sedimentological and chemical input

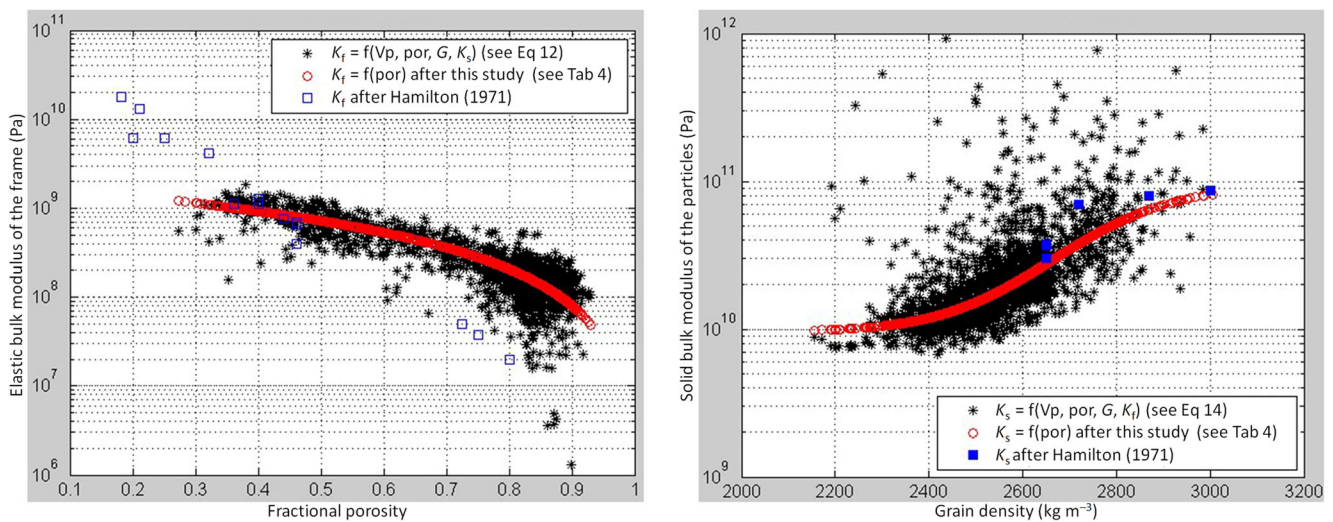


Fig. 7 Elastic frame bulk modulus vs. porosity (*left*), and solid grain bulk modulus vs. grain density (*right*), with corresponding fitting functions (*red circles*). *Blue squares* Values obtained from the literature (see main text for more information)

parameters, i.e. water content, LOI, grain density, grain size parameters (mean, sorting, skewness) after Folk (1954, 1966), number of modes in grain size distributions (uni-, bi- or trimodal), and XRF element scans (Al, Si, S, K, Ca, Ti, Mn, Fe, Zr, Ba). Cluster analysis was by the method of Ward (1963), with the Euclidean distance measure using the z-score standardised data. Thereby, four classes were identified. The allocation to the classes was adjusted by discriminant analysis, and the resulting class membership probabilities proved the non-ambiguity of classification for each sample where 100% of the classified samples could be allocated with 0.9 (membership probability) to its particular class. The discriminant analysis likewise was the basis for Fig. 11

by interpolating the membership probabilities of each class separately at UTM33 coordinates for isometry. Their distribution patterns are shown in Fig. 11 and reflect mainly bathymetric information, although bathymetry was not a parameter for the cluster analysis.

In all, 229 of the 252 sampling stations were selected for classification; the remaining 23 stations lacked at least one parameter. Based on this classification, one sample was exemplarily chosen from each of the four classes for mineralogical analyses by means of SEM/EDX, with results shown in Table 6.

On average the samples are clay mineral dominated (illite + illite-mixed layer 32.9%±4.7, smectite 4.6%±0.9, chlorite 2.7%±0.2, kaolinite 1.1%±0.2), and contain 23.9%±1.7

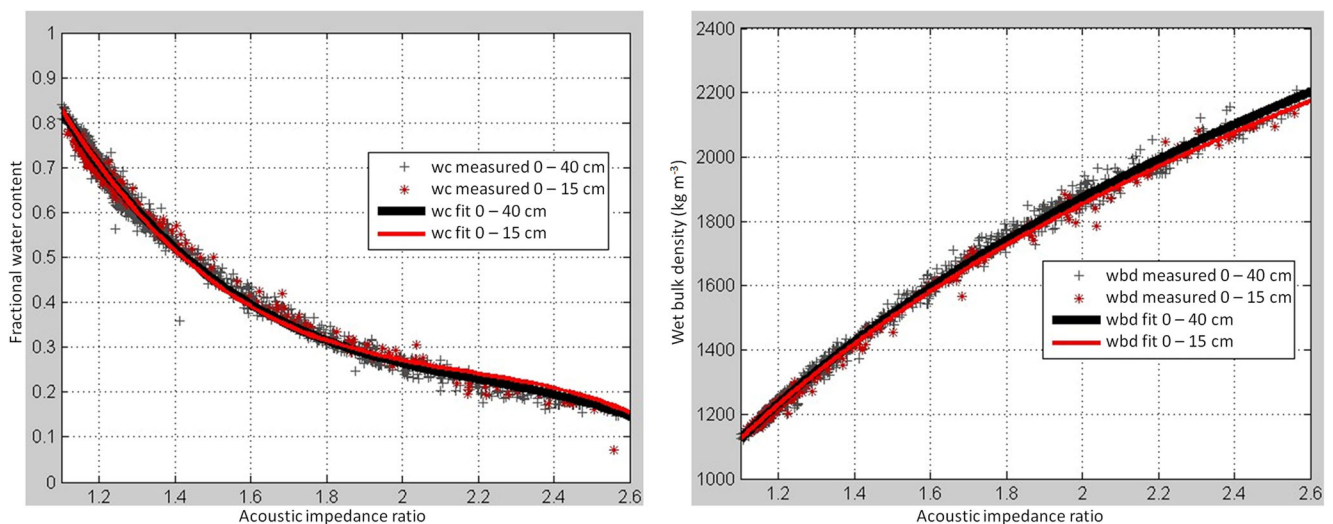


Fig. 8 Fractional water content *wc* (*left*) and wet bulk density *wbd* (*right*) as functions of the acoustic impedance ratio *ZR*

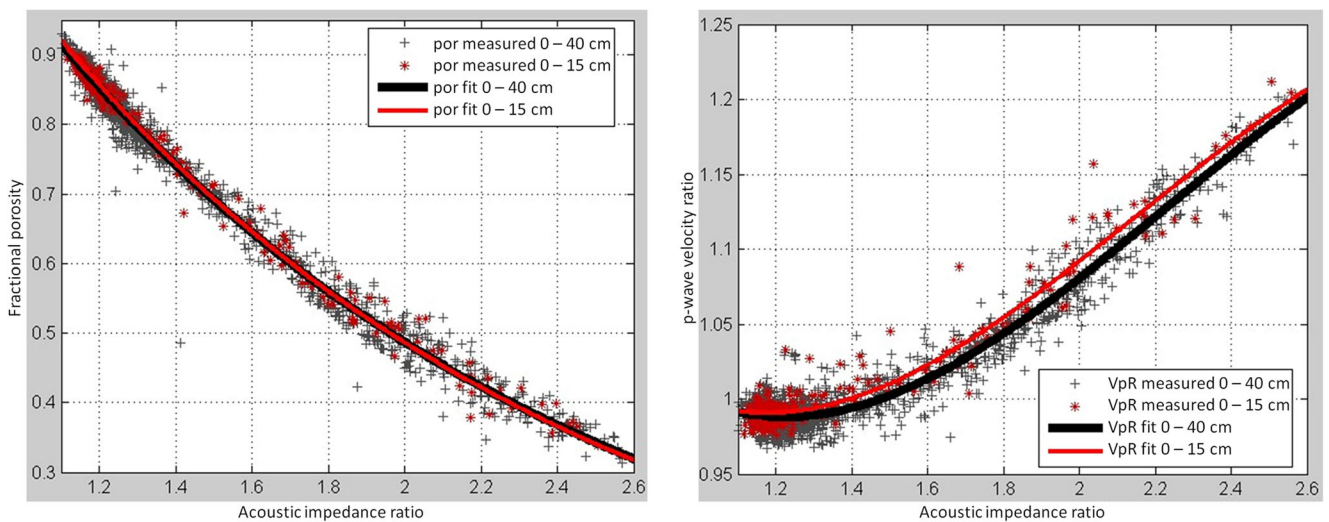


Fig. 9 Fractional porosity por (*left*) and p-wave velocity ratio VpR (*right*) as functions of the acoustic impedance ratio ZR

quartz, $8.2\% \pm 1.0$ potassic feldspar, $6.8\% \pm 0.5$ albite and $4.7\% \pm 1.0$ opal. The most common *class 4* (95 stations) and *class 3* (63 stations) represent basin sediments with high LOI values of about 0.13 ($\approx 5\%$ TOC) and accordingly elevated water contents (69%), increased sulphur XRF counts, lower grain density (2.5 g cm^{-3}) and medium silt (median=12 μm). What distinguishes these two classes is the higher amounts of opal (6%), calcite (2.2%) and dolomite (1.3%) in class 3, and the increased pyrite (2.8%) in class 4.

Class 2 (31 stations) comprises coastal areas with coarser sediments, i.e. medium sand (median 300 μm), and accordingly lower water content (20%), less clay minerals (e.g. illite 26.2%), lowest pyrite (0.5%), elevated FePO_4 (1.3%) and a remarkable maximum of Fe-oxides (9.4%)—the other classes have values clearly below 2%. *Class 1* (13 stations) is

characterised by transitional sediments having intermediate values for almost all parameters. The median grain size is 78 μm , i.e. fine sand with LOI values of 0.03 ($\approx 1\%$ TOC) and 30% water content.

Fig. 11 these classes are shown as continuous colours ranging from brown (class 4) to light yellow (class 1). The classified sampling stations are identified by their class numbers. Moreover, all stations have circles showing their acoustical impedance ratios (including those that could not be classified; cf. above) in colours similar to those used for the four classes (values grouped at geometric scale), i.e. mismatch between sediment classification and acoustical impedance would be visible where, for example, a brown circle lies upon a green background. Comparison of the two basins reveals a slightly higher grain density in the Arkona Basin ($2.61 \pm 0.097 \text{ g cm}^{-3}$)

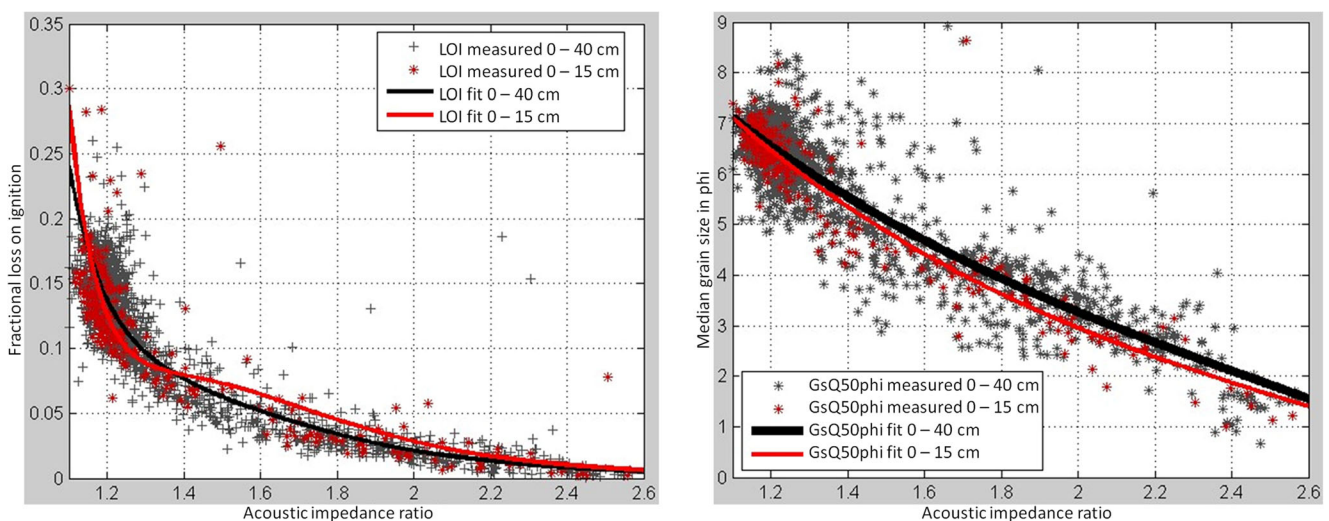


Fig. 10 Fractional loss on ignition LOI (*left*) and median grain size $GsQ50phi$ (*right*) as functions of the acoustic impedance ratio ZR

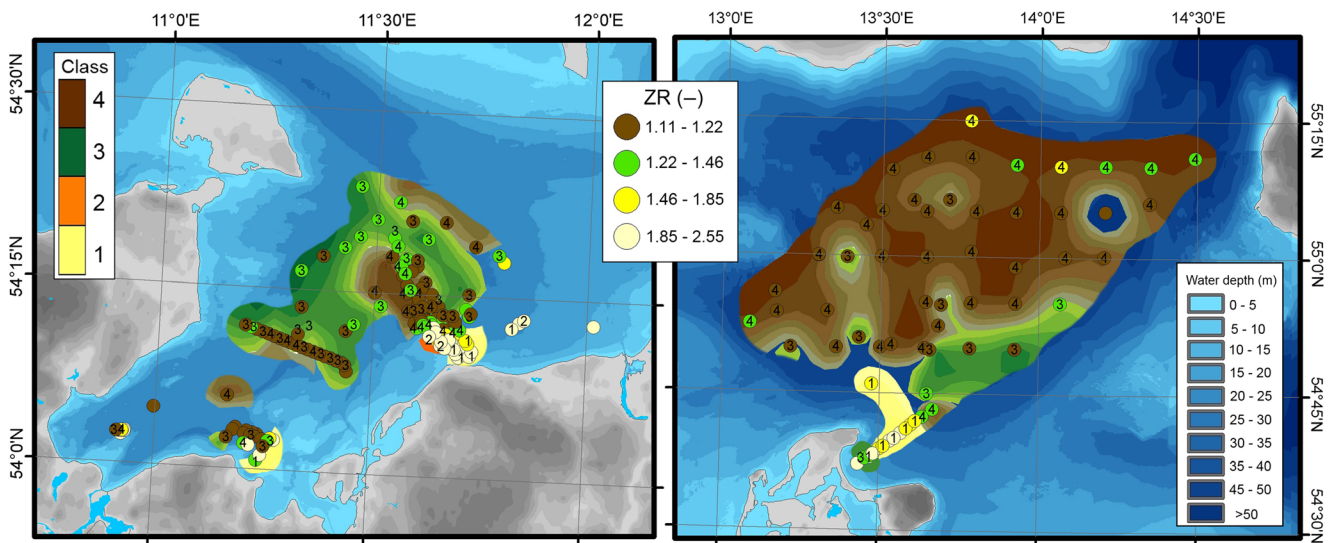


Fig. 11 Sediment classes 1 to 4 and associated acoustic impedance ratio for Mecklenburg Bay (left) and the Arkona Basin (right). Values in circles Class numbers, background colours interpolated classes, colours within

circles ZR values. Note the different geographical scales of the two basins. For more information, see main text

Table 6 Chemical and sedimentological data on four representative sub-samples characterising the four sediment classes

Station (IOW)	283840	283990	283970	303070
Cluster no.	1	2	3	4
Sum clay minerals (%)	43.75	35.39	42.33	46.76
Illite-mixed layer (%)	29.05	21.39	26.72	27.75
Illite (%)	6.61	4.80	6.40	8.71
Smectite (%)	3.33	4.65	5.02	5.37
Chlorite (%)	2.91	2.58	2.53	2.61
Kaolinite (%)	0.97	1.16	0.79	1.32
Saponite (%)	0.88	0.80	0.86	1.01
Quartz (%)	25.93	23.38	24.33	21.91
Opal (%)	4.88	4.18	6.05	3.75
Sum feldspars (%)	17.59	15.73	17.30	19.39
Potassic feldspar (%)	8.83	7.18	7.49	9.19
Albite (%)	6.47	6.43	6.58	7.52
Plagioclase (%)	2.29	2.12	3.23	2.68
Calcite (%)	0.92	1.91	2.19	1.75
Dolomite (%)	0.95	0.41	1.28	0.48
Pyrite (%)	0.76	0.52	1.53	2.76
Titanium minerals (%)	1.55	1.76	1.09	1.16
Fe-oxides (%)	1.48	9.35	1.74	0.55
CaPO ₄ (%)	0.35	0.67	0.56	0.53
FePO ₄ (%)	0.30	1.27	0.35	0.04
LOI (-)	0.03	0.01	0.12	0.13
wc (-)	0.30	0.20	0.69	0.69
d _s (kg m ⁻³)	2,699	2,689	2,516	2,552
Median grain size (µm)	78	304	12	12

compared to Mecklenburg Bay ($2.54 \pm 0.137 \text{ g cm}^{-3}$), which does not result from lower LOI in the Arkona Basin (both basins have LOI values of about 11%, i.e. about 4% TOC).

Discussion and conclusions

The use of empirical functions is the most simple and straightforward method for the establishment of geo-acoustic models in a specific depositional environment. The results of the regression analyses provide a useful set of equations for the calculation of acoustic surface sediment properties with a reasonable fitting error for most practical applications. The Baltic Sea results are in good agreement with the regressions of Jackson und Richardson (2007) for various settings worldwide (see Fig. 6 left panel, blue versus turquoise lines).

In contrast to regression functions specific for a depositional environment, physically based models in general do not have spatial limitations. Nevertheless, their application requires a number of input parameters, some simple to measure, others not and needing to be derived from measured parameters. An applicable version of the models of Gassmann (1951) and Hamilton (1971a, 1971b, 1980) was developed and used in this paper for the prediction of in situ p-wave velocity from sedimentological parameters, i.e. fractional water content, grain density and the desired in situ environmental parameters S, T, P. The most challenging problem was to find suitable functions for the calculation of the elastic bulk moduli of the frame K_f and of the solid particles K_s from available sedimentological parameters—in this case, fractional porosity and grain density.

Since the Gassmann-Hamilton approach contains an empirical part for the prediction of K_f and K_s , its theoretical advantage of being a physical model over the regression model cannot be proven. At least the in situ correction via pore water properties (K_w) is more straightforward in the physical model. However, both the present regression model and the Gassmann-Hamilton model can be used as tools for the prediction of surface sediment acoustic properties with remarkably good performance in the south-western Baltic Sea.

It is very likely that the Gassmann-Hamilton model can be used with the same performance for p-wave predictions of surface sediments in other regions. The p-wave velocity ratio (VpR) is normalised to environmental conditions, compensating the influence of salinity and temperature to make values comparable. To calculate the desired p-wave velocity for a given set of temperature (T), pressure (P) and salinity (S), VpR should be multiplied with the p-wave velocity of the pore water $V_{pw}(S,T,P)$. The regression analyses of the p-wave velocity ratio (Figs. 4 and 5, Table 3) show the expected strong dependencies on fractional water content, wet bulk density, loss on ignition and median grain size with fitting errors of about 17–32 m s⁻¹. The similarity of the regression lines reflects the high degree of correlation between these variables.

The most critical input parameters are K_s and K_f , the compression moduli of the solid particles and of the solid frame. Knowing the mineral composition, most authors calculated K_s as a kind of weighted mean from K_s mineral values (Hamilton 1971a; Stoll 1974, 1989). The basic dataset used is compiled from samples of different depositional settings. The solid matter composition varies from quartz- and feldspar-dominated fine sand (basin margin) to silt with more clay minerals and high organic contents (centre of the basins). Nevertheless, more precise information is required about the effects of mineral composition. Also, the influence of different organic matter contents on the compression modulus of the solid particles K_s is still unknown. Likewise, Hamilton (1971a) published K_f vs. porosity relations derived from drained static compression tests for sand, silt and clays but attempts to use his formula together with the above K_s assumptions as input for the Gassmann-Hamilton model were not satisfactory.

Acoustic profiling techniques widely employed for seafloor mapping (cf. review by Anderson et al. 2008) include the usage of seafloor echo amplitude of single-beam echosounders for sediment classification (e.g. Richardson and Briggs 1993; Du and Chen 2007; Snellen et al. 2011). One of the key problems to solve is the extraction of the plane wave reflection coefficient from the acoustic seafloor echo, which can be considered as a superimposition of backscatter and reflective components. This aspect exceeds the topic of the present paper, in which the acoustic impedance of seafloor sediments was calculated from the plane wave reflection coefficient determined on sub-samples, and its relations to physical and sedimentological parameters analysed by regression.

As acoustic impedance is the product of p-wave velocity and wet bulk density, an analytic solution is possible only if one of these parameters is known. The very promising results of the regression analyses (Figs. 8, 9, 10, Table 5), with fitting errors of about 0.01 for the fractional water content, about 20 kg m⁻³ for wet bulk density and less than 20 m s⁻¹ for the p-wave velocity, confirm the suitability of this method. The good performance can be explained by the strong correlation of wet bulk density and p-wave velocity (Fig. 8, left panel), in turn well correlated to other properties. The sediment dataset from the inner basin sectors can be distinguished from the nearshore dataset in terms of not only grain size spectra but also mineralogical composition and associated water content, in turn linked with acoustic parameters. For a given acoustic impedance ratio, specific sedimentological parameters can be calculated using the formulae of Table 5.

Combining evaluations of interrelations between physico-chemical sediment parameters and acoustic impedance, the extended classification method of the present study considerably expands on earlier attempts at sediment classification in the western Baltic Sea based on grain size parameters (e.g. Figge 1981; Tauber and Lemke 1995; Bobertz and Harff 1999, 2004; Bobertz et al. 2006; Tauber and Seifert 2010; Tauber 2012). Acoustically relevant parameters such as w_c and d_s are also included in this classification, although only as two of 17 equally weighted variables. The data reveal water content as a key factor in defining sediment classes. High water contents of muddy sediments in the centre of the basins are associated with low acoustic impedances, the reverse being the case for coastal areas with sandy sediments. The pattern is clearer for the Arkona Basin than for Mecklenburg Bay, likely due to the proximity to the fissured coast and shallower water depths in the latter where the action of currents and waves would result in more heterogeneous sediment composition. Moreover, classification derived solely on the basis of acoustic impedance results in different distribution patterns than when derived from sedimentological and geochemical parameters. This indicates that the latter parameters are not directly coupled to the acoustic impedance. This needs to be considered in future acoustic seafloor classifications.

In conclusion, semi-empirical equations for the calculation of the elastic frame modulus and the solid sediment particle modulus established by an iterative Gassmann-Hamilton fitting procedure resulted in a remarkable improvement in model accuracy for seafloor sediments from Mecklenburg Bay and the Arkona Basin in the south-western Baltic. Only water content, grain density and the desired environmental conditions (S,T,P) are required for the prediction of in situ p-wave velocity, wet bulk density and acoustic impedance. In turn, selected seafloor sediment parameters can be derived from seafloor acoustic reflectivity with about the same precision, forming a solid base for the effective mapping of acoustic seafloor sediment

properties such as water content, wet bulk density and sound velocity. These findings can serve in upgrading to a Biot-based model, where crucial input parameters such as the elastic moduli (K_s and K_f) can now be calculated on the basis of sedimentological properties with more confidence. Moreover, they can aid in future attempts to establish precise linkages between sediment facies identified in longer cores (up 12 m) and corresponding acoustic facies recorded by high-resolution seismic profiling, notably incorporating the effect of compaction for Baltic Sea sediments and, for that matter, similar settings in other world regions.

Acknowledgements This study was carried out within the framework of the IS-Sedilab (In Situ Sediment Laboratory) project funded by the German Federal Ministry of Education and Research (grant no. 03F0630). Older data and sediment samples were taken from former projects also funded by the German Federal Ministry of Education and Research: BONUS - BALTIC GAS (grant no. 03F0488B), and DYNAS (Dynamics of Natural and Anthropogenic Sedimentation, grant no. 03F0280A). The authors acknowledge constructive comments from C. Hass, an anonymous reviewer and the journal editors.

References

- Anderson JT, Holliday DV, Kloser R, Reid DG, Simard Y (2008) Acoustic seabed classification: current practice and future directions. *ICES J Mar Sci* 65:1004–1011
- Andrén E, Andrén T, Sohlenius G (2000) The Holocene history of the southwestern Baltic Sea as reflected in a sediment core from Bornholm Basin. *Boreas* 29:233–250
- Bartholomä A (2006) Acoustic bottom detection and seabed classification in the German Bight, southern North Sea. *Geo-Mar Lett* 26:177–184
- Biot MA (1956a) Theory of propagation of elastic waves in a fluid-saturated porous solid I. Low-frequency range. *J Acoust Soc Am* 28:168–178
- Biot MA (1956b) Theory of propagation of elastic waves in a fluid-saturated porous solid II. Higher frequency range. *J Acoust Soc Am* 28:179–191
- Biot MA (1962) Generalized theory of acoustic propagation in porous dissipative media. *J Acoust Soc Am* 34:1254–1265
- Blum P (1997) Physical Properties Handbook: a guide to the shipboard measurement of physical properties of deep-sea cores. ODP Tech Note 26
- Bobertz B, Harff J (1999) Mapping the sedimentary facies of marginal seas using regionalized classification. In: Proc IAMG'99, 5th Annu Conf International Association for Mathematical Geology, 6–11 August 1999, Trondheim, pp 135–138
- Bobertz B, Harff J (2004) Sediment facies and hydrodynamic setting: a study in the south western Baltic Sea. *Ocean Dynam* 54:39–48
- Bobertz B, Harff J, Kramarska R, Lemke W, Przedziecki P, Uszinowicz S, Zachowicz J (2006) Surface sediments of the south-western Baltic Sea. Gdansk, Polish Geological Institute, Baltic Sea Research Institute Warnemünde
- Chotiros NP, Isakson MJ (2004) A broadband model of sandy ocean sediments: Biot-Stoll with contact squirt flow and shear drag. *J Acoust Soc Am* 116:2011–2022
- DIN18124 (2011) Baugrund, Untersuchung von Bodenproben - Bestimmung der Korndichte - Kapillarpkyknometer, Weithalspyknometer, Gaspyknometer. Deutsches Institut für Normung eV (DIN), April 2011, Beuth Verlag, Berlin
- Du D, Chen Y (2007) Investigation of the relationship between seafloor echo strength and sediment type—a case study in Jiaozgou Bay, China. *Geo-Mar Lett* 27:339–344
- Dvorkin J, Nur A (1993) Dynamic poroelasticity: a unified model with the squirt and the Biot mechanism. *Geophysics* 58:524–533
- Endler R (2009) Sediment physical properties of the DYNAS study area. *J Mar Systems* 75:317–329
- Eronen M, Ristaniemi O, Lange D (1990) Analyses of a sediment core from the Mecklenburg Bay, with a discussion on the early Holocene history of the southern Baltic Sea. *Geol Foren Forhandl (Stockholm)* 112(1):1–8
- Figge K (1981) Sedimentverteilung in der Deutschen Bucht Maßstab 1: 250000. Deutsche Hydrographische Institut, Hamburg, Karte Nr. 2900
- Folk RL (1954) The distinction between grain size and mineral composition in sedimentary rock nomenclature. *J Geol* 62(4):344–359
- Folk RL (1966) A review of grain-size parameters. *Sedimentology* 6:73–93
- Gassmann F (1951) Elastic waves through a packing of spheres. *Geophysics* 16(4):673–685. doi:10.1190/1.1437718
- Hamilton EL (1971a) Elastic properties of marine sediments. *J Geophys Res* 76:579–604
- Hamilton EL (1971b) Prediction of in-situ acoustic and elastic properties of marine sediments. *Geophysics* 36:266–284
- Hamilton EL (1980) Geoacoustic modeling of the sea floor. *J Acoust Soc Am* 68(5):1313–1340
- Hamilton EL, Bachman RT (1982) Sound velocity and related properties of marine sediments. *J Acoust Soc Am* 72:1891–1904
- Hamilton EL, Shumway G, Menard HW, Shippek CJ (1956) Acoustic and other physical properties of shallow-water sediments off San Diego. *J Acoust Soc Am* 28:1–15
- Jackson DR, Richardson MD (2007) High-frequency seafloor acoustics. Springer, New York
- Jensen JB (1995) A Baltic Ice Lake transgression in the southwestern Baltic: evidence from Fakse Bugt, Denmark. *Quat Int* 27:59–68
- Jensen JB, Bennike O, Witkowski A, Lemke W, Kuijpers A (1997) The Baltic Ice Lake in the southwestern Baltic: sequence-, chrono- and biostratigraphy. *Boreas* 26:217–236
- Krauss W, Brüggge B (1991) Wind-produced water exchange between the deep basins of the Baltic. *J Phys Oceanogr* 21:373–384
- Krumbein WC (1938) Size frequency distributions of sediments and the normal phi curve. *J Sediment Petrol* 8:84–90
- Lass HU, Mohrholtz V (2003) On dynamics and mixing of inflowing saltwater in the Arkona Sea. *J Geophys Res* 108(C2):3042. doi:10.1029/2002JC001465
- Leipe T, Löffler A, Bahlo R, Zahn W (1999) Automated particle analysis of water samples by scanning electron microscopy and X-ray microanalysis. *Vom Wasser* 93:21–37
- Leipe T, Tauber F, Vallius H, Kabel Virtasalo JJ, Uścińowicz S, Kowalski N, Hille S, Lindgren S, Myllyvirta T (2011) Particulate organic carbon (POC) in surface sediments of the Baltic Sea. *Geo-Mar Lett* 31:175–188
- Lemke W (1998) Sedimentation und paläogeographische Entwicklung im westlichen Ostseeraum (Mecklenburger Bucht bis Arkona Becken) vom Ende der Weichselvereisung bis zur Litorinatransgression. Marine Science Reports Institut für Ostseeforschung - Baltic Sea Research Institute Warnemünde, Germany, vol 31
- Leurer KC (1997) Attenuation in fine-grained marine sediments: extension of the Biot-Stoll model by the “effective grain model” (EGM). *Geophysics* 62:1465–1479
- Liljebadh B, Stigebrandt A (1996) Observations of the deepwater flow into the Baltic Sea. *J Geophys Res* 101(C4):8895–8911

- Lu T, Bryant WR, Slowey NC (1998) Regression analysis of physical and geotechnical properties of surface marine sediments. *Mar Georesources Geotechnol* 16:201–220
- Lurton X (2002) An introduction to underwater acoustics, principles and applications. Springer, Berlin
- Manheim FT, Dwight L, Belastock RA (1974) Porosity, density, grain density, and related physical properties of sediments from the Red Sea drill cores. In: DSDP Initial Report vol XXIII part 3, chap 26, pp 887–907
- Mavko G, Mukerji T, Dvorkin J (1999) The rock physics handbook: tools for seismic analysis in porous media. Cambridge University Press, Cambridge
- Mendoza U, Neto AA, Abuchacra RC, Barbosa CF, Figueiredo AG, Gomes MC, Belem AL, Capilla R, Albuquerque ALS (2014) Geoacoustic character, sedimentology and chronology of a cross-shelf Holocene sediment deposit off Cabo Frio, Brazil (southwest Atlantic Ocean). *Geo-Mar Lett* 34:297–314
- Miltner A, Emeis K-C (2000) Origin and transport of terrestrial organic matter from the Oder lagoon to the Arkona Basin, Southern Baltic Sea. *Org Geochem* 31:57–66
- Mogollón JM, Dale AW, Jensen JB, Schlüter M, Regnier P (2013) A method for the calculation of anaerobic oxidation of methane rates across regional scales: an example from the Belt Seas and The Sound (North Sea–Baltic Sea transition). *Geo-Mar Lett* 33:299–310
- Morgan PP (1998) Seawater. A library of MATLAB computational routines for the properties of seawater. <http://www.marine.csiro.au/>, accessed 4 November 2013
- Olea R, Bobertz B, Harff J, Endler R (2008) Enhancement of seafloor maps for Mecklenburg Bay, Baltic Sea using proxy variables. In: Bonham-Carter GF, Cheng Q (eds) *Progress in geomathematics*. Springer, Berlin, pp 457–480
- Orlowski A (2007) Acoustic seabed classification applied to Baltic benthic habitat studies: a new approach. *Oceanologia* 49(2):229–243
- Ostrovsky I, Tegowski J (2010) Hydroacoustic analysis of spatial and temporal variability of bottom sediment characteristics in Lake Kinneret in relation to water level fluctuation. *Geo-Mar Lett* 30: 261–269
- Parnum I, Siwabessy J, Gavrilov A, Parsons M (2009) A comparison of single beam and multibeam sonar systems in seafloor habitat mapping. In: *Proc 3rd Int Conf Exhib Underwater Acoustic Measurements: Technologies and Results*, 21–26 June 2009, Kos, Greece
- Richardson MD, Briggs KB (1993) On the use of acoustic impedance values to determine sediment properties. In: *Acoustic Classification and Mapping of the Seabed*, Underwater Acoustics Group Conf, 14–16 April 1993, University of Bath, Proc Institute of Acoustics, vol 15, part 2, pp 15–25
- Richardson MD, Bryant WR (1996) Benthic boundary layer processes in coastal environments. *Geo-Mar Lett* 16:133–278
- Schwartz BM (1985) Grain density measurements of ash flow tuffs: an experimental comparison of water immersion and gas intrusion pycnometer techniques. Sandia National Laboratories, Albuquerque, NM, report SAND 83-1327
- Snellen M, Siemes K, Simons DG (2011) Model-based sediment classification using single-beam echo sounder signals. *J Acoust Soc Am* 129:2878–2888
- Stoll RD (1974) Acoustic waves in saturated sediments. In: Hampton L (ed) *Physics of sound in marine sediments*. Plenum Press, New York, pp 19–39
- Stoll RD (1989) *Sediment acoustics*. Springer, Berlin
- Tauber F (2012) *Meeresbodenrelief in der deutschen Ostsee*. Map 1:100 000. Bundesamt für Seeschifffahrt und Hydrographie, Hamburg
- Tauber F, Lemke W (1995) Map of sediment distribution in the Western Baltic Sea (1:100,000), Sheet “Darß”. *Ocean Dynam* 47(3):171–178
- Tauber F, Seifert T (2010) Relief map of the Baltic Sea. In: Vlasov N (ed) *HELCOM Atlas of the Baltic Sea*. Baltic Marine Environment Protection Commission - Helsinki Commission, no 25
- Tegowski J (2005) Acoustical classification of the bottom sediments in the southern Baltic Sea. *Quat Int* 130:153–161
- Ulyanova M, Sivkov V, Kanapatskij T, Pimenov N (2014) Seasonal variations in methane concentrations and diffusive fluxes in the Curonian and Vistula lagoons, Baltic Sea. *Geo-Mar Lett* 34:231–240
- Ward JH (1963) Hierarchical grouping methods to optimize an objective function. *J Am Stat Assoc* 58:236–244
- Wöfl A-C, Lim CH, Hass HC, Lindhorst S, Tosonotto G, Lettmann KA, Kuhn G, Wolff J-O, Abele D (2014) Distribution and characteristics of marine habitats in a subpolar bay based on hydroacoustics and bed shear stress estimates—Potter Cove, King George Island, Antarctica. *Geo-Mar Lett* 34:435–446
- Yang Y (2004) Measuring mudstone properties in the laboratory. BP best practice Pro Quant Consultants. <http://www.igutexasedu/people/staff/flemings/tutorials/tech/MeasuringMudstoneProperties.pdf>, accessed 6 February 2012